Chemical Micromotors Move Faster at Oil-Water Interfaces

Jiayu Liu[1], Zhou Yang[1], Zuyao Yan[1], Shifang Duan[1], Xiaowen Chen[1], Donghao Cui[1], Dezhou Cao[1], Ting Kuang[2], Xing Ma[1,3], Wei Wang[1]*

1 School of Materials Science and Engineering, Harbin Institute of Technology (Shenzhen), Shenzhen, China, 518055

2 Education Center of Experiments and Innovations, Harbin Institute of Technology (Shenzhen), Shenzhen, China, 518055

3 Sauvage Laboratory for Smart Materials, Harbin Institute of Technology (Shenzhen), Shenzhen, China, 518055

KEYWORDS Oil-water interface, Micromotor, Speed increase, Faster chemical reaction, Tilt angle

ABSTRACT: Many real-world scenarios involve interfaces, particularly liquid-liquid interfaces, that can fundamentally alter the dynamics of colloids. This is poorly understood for chemically active colloids that release chemicals into their environment. We report here the surprising discovery that micromotors—colloids that convert chemical fuels into self-propulsion—move significantly faster at an oil-water interface than on a glass substrate. Typical speed increases ranged from 3-6 times up to an order of magnitude, and were observed for different types of chemical motors or oils. Such speed increases are likely caused by faster chemical reactions at an oil-water interface than a glass-water interface, but the exact mechanism remains unknown. Our results provide valuable insights into the complex interactions between chemical micromotors and their environments, which are important for applications in the human body or in the removal of organic pollutants from water. In addition, this study also suggests that chemical reactions occur faster at an oil-water interface, and that micromotors can serve as a probe for such an effect.

INTRODUCTION

Micromotors that can convert external energy into autonomous motion hold great promise as the core platform for next-generation autonomous, multifunctional microrobotics.[1-3] Applications range from minimally invasive surgery[4] and drug delivery and biosensing[5] to environmental remediation,[6] defense and security,[7] and bottom-up micromachine assembly.[8] In these applications exist various types of confinement, such as solid-liquid, liquid-liquid, and liquid-gas interfaces, that could significantly alter the individual and collective dynamics of microrotors.[9, 10] Understanding the dynamics of micromotors in such complex environments thus holds applied importance, and could in turn reveal intricate details of how micromotors operate, as well as the physico-chemical details of an interface.

Compared with other types of interfaces, micromotors moving on liquid-liquid interfaces are less explored and understood. These interfaces can be found in environmental remediatiat and in biological samples. There, the dynamics of a micromotor can be changed by the unique interfacial properties such as a sharp change in viscosity and in chemical composition, and flows driven by interfacial tension gradients. This is especially the case for micromotors powered by chemical reactions, and in particular by chemical gradients.[11-15] For example, Dietrich et al.[16] found that when a chemical micromotor was embedded in an oil-water interface, the reorientation of its Janus face led to two peaks in its speed distributions. Simmchen and Kretzschmar[17] found that an oil-water interface can bring the tilt angle of a chemical micromotor close to 90° with the interface. Moreover, Simmchen and Sanchez et al.[18, 19] found that an oil-water interface trapped and guided chemical micromotors in a way similar to a solid boundary.

In this article, we report that chemically powered micromotors move several times faster than those moving on a glass-water interface. Typical speed increases were 3-6 fold, but speed increase of one order of magnitude was also frequently observed. The robustness of this observation of speed increase is confirmed with multiple types of chemically powered micromotors, and confirmed with different types of oils. We propose that the speed increase reported arises primarily from faster chemical reactions rates at an oil-water interface, an effect confirmed by a few pieces of experimental evidence.

Our discovery of the fast speeds of chemical micromotors at oil-water interfaces reveals interesting dynamics of micromotors in confined environments, where reaction kinetics, distributions of physico-chemical fields and flows are intricately coupled. Such a speed increase can inspire faster micromotor designs of better energy efficiency, which is particularly useful for environmental remediation, micro-mixing or food processing applications that involve oil-water emulsions. In addition, chemical micromotors could serve as a local probe for the reaction rate at an oil-water interface, providing real-time, visual, and

quantifiable monitoring of interfacial reaction kinetics that are both important and elusive.

EXPERIMENTAL SECTION

Materials and Instruments. Hydrogen peroxide (H_2O_2, 30 wt. %) and Ag plating solutions (#44067) were purchased from Alfa Aesar. Rh plating solution (#290255GL) were purchased from Technic Inc. Au plating solution was self-made. Ethanol (CH_3CH_2OH, 99.5%), isopropyl alcohol (C_3H_8O, 99.5%), cyclohexane (C_6H_{12}, 99.5%), tetrabutyl titanate (TBT, T104105, 99%), ascorbic acid ($C_6H_8O_6$, 99%), Arabic gum, potassium chloride (KCl, 99.5%), Rhodamine B (RB, 99%), Nile Red (95%), D-(+)-Glucose (99.5%), sodium tungstate ($Na_2WO_4{\cdot}2H_2O$), triethanolamine (TEOA, 99%), hydroquinone (H_2Q, 99%), decane ($C_{10}H_{22}$), dibutyl phthalate, perfluorooctane (C_8F_{18}), and silicone oil (PMX-200) were purchased from Aladin, China. Novec HFE 7100 was purchased from 3M, USA. PFPE-PEG-PFPE fluorosurfactant was purchased from Creative PEGWorks. Phenylated Silicone oil (KF-54) was purchased from Shin-Etsu Chemical Co., Ltd. Trichloro (octadecyl) silane (OTS, 104817, 90%) and silver nitrate ($AgNO_3$, 99%) were purchased from sigma. Lutensol To-7 (9043-30-5, 99%) was purchased from Shandong Usolf Chemical Technology Co., Ltd of China. Chloroauric acid ($HAuCl_4$ $4H_2O$, 47.8%) was purchased from Sinopharm Chemical Reagent Co. Ltd of China. The hydrogen peroxide assay kit (Biochemical Assay Kit, #E-BC-K102-S) was purchased from Elabscience. All chemicals were used without further purification.

Silica (SiO_2) microspheres were purchased from Tianjin Baseline Chromtech Research Center, China. The polystyrene (PS) microspheres were procured from Shanghai Huge Biotechnology Co., Ltd of China. Glass cover slips were purchased from Deckglaser (#0101050, 22×22 mm, No.1), which were made of chemically resistant borosilicate glass D 263® M of the first hydrolytic class. Prior to use, the glass cover slips were sequentially subjected to a 5-minute ultrasonic cleaning in ethanol and isopropanol, followed by drying with nitrogen gas (N_2). Subsequently, they were subjected to a 5-minute ultrasonic cleaning in deionized water (18.2 MΩ cm) and dried with N_2. The dried glass cover slips were then stored in a dry glass container for future use. Unless otherwise noted, these cover slips with a contact angle of ~ 20°will be used as the "glass substrates" in our experiments.

An Olympus IX73 inverted optical microscope and a Point Gray camera (FL3-U3-13E4C-C) were utilized for the observation of experimental phenomena and the recording of experimental data. A high vacuum sputter machine (Leica EM ACE600) was used to coat platinum, gold or silver onto microspheres. A low vacuum sputter machine (Ky Technology; SBC-12) were used to coat platinum oxide onto silica microspheres. A field-emission scanning electron microscope (FESEM; Zeiss SUPRA 55) and a confocal laser scanning microscope (Leica SP8 X) were used for imaging. UV-Vis spectroscopy was characterized by Shimadzu UV-3600. The zeta potential of the oil phase was determined by the Zetasizer NanoZS90 through measuring the ultrasonically dispersed oil droplets in deionized water. The dissolved oxygen content in the water was measured using the HQ30d Portable Meter Kit with LDO101 (Hach). The conductivity of the KCl solution was measured using the S470 conductivity meter from Mettler Toledo.

Preparation of various Janus microspheres. TiO_2 microspheres were synthesized through a core–shell method[20] that we reported earlier. Au microspheres were chemically synthesized following a previous publication.[21] WO_3 microspheres were synthesized based on ref. 22. To make Janus microspheres, isotropic microspheres were suspended in 20 μL of ethanol and dispersed using ultrasound. Subsequently, the suspensions were deposited onto a small piece of clean silicon wafer to form monolayers. Most of Janus micromotors, including SiO_2-Pt, PS-Pt, TiO_2-Pt, WO_3-Pt and Au-Pt types, were made by sputtering a thin layer of Pt (~20 nm) onto one side of microsphere monolayers in a chamber prefilled with argon, at a vacuum level of 6.77×10^{-3} Torr with a high vacuum sputter coater. Following ref. 23 5 μm PS-Ni-Pt Janus microspheres were made by evaporating a 15 nm Ni layer before the Pt coating. SiO_2-PtO Janus micromotors were prepared by sputtering Pt of ~20 nm on a monolayer of SiO_2 spheres in a chamber filled with air, at a vacuum level of 3.8×10^{-2} Torr with a low vacuum sputter coater. Janus SiO_2-Ag microspheres were fabricated by evaporating a 50 nm layer of Ag onto the monolayer of SiO_2 microspheres via electron beam evaporation (TF500, HHV). Silver was converted into silver chloride by immersing the silicon wafer carrying the Janus SiO_2-Ag microsphere monolayer into $FeCl_3$ solutions (0.01 mol/L, at room temperature for 20 min), following ref. 24. The resulting Janus microspheres of each type were dispersed in deionized water after sonication.

Preparation of hydrophilic or hydrophobic glass substrates. Hydrophobic glass substrates were prepared by solution deposition of OTS on glass. Prior to deposition, the glass coverslips were cleaned using isopropyl alcohol and then deionized water. Subsequently, the cleaned glass substrates were treated for 3 minutes with air plasma of radio frequency power of 3.0 MHz and an output power of 29.6 W. OTS was deposited by immersing a clean glass substrate in a freshly prepared 0.228 mM OTS solution in cyclohexane for 12 h in a sealed glass bottle. The silanized substrates were sonicated sequentially in cyclohexane, isopropyl alcohol and deionized water and then dried in nitrogen. Finally, the silanized substrates were stored in petri dishes sealed with Parafilm and placed in a desiccator for no more than 3 days before use.

Hydrophilic glass substrates were prepared by treating a glass substrate for 200 seconds in a plasma cleaner (MTI plasma cleaner, PCE-6). The radio frequency power was 3.0 MHz and the output power was 29.6 W. The wettability of the processed glass substrate was characterized by measuring the contact angles of deionized water using a contact angle goniometer (POWEREACH, JC2000D1).

Construction of oil-water interfaces and glass-water interfaces. After retrieving a hydrophobic glass substrate from a sealed petri dish, a 2 mm thick 3M silicone gasket with a hole of a diameter of 5 mm was attached onto the

hydrophobic side of the substrate. Then, 20 μL of oil was added into the chamber. Unless otherwise specified, oil-water interfaces in this work were all constructed with silicone oils of a viscosity of 1000 mPa·s. After the oil phase stabilized, 4 μL of deionized water containing motors was added into the chamber. After the motors settled completely near the oil-water interface, 4 μl of fuel or deionized water was added to keep the volume of the water phase above the oil-water interface at 8 μl. Due to the hydrophobicity of the substrate, a stable and continuous oil-water interface was formed, with the water phase staying on the top and the oil phase on the bottom. The same protocol was used for preparing a glass-water interface except that an untreated or hydrophilic glass cover slip was used instead of a hydrophobic one. Note that the oil-water interface could partially collapse over time due to the higher density of the water phase. This was exploited for the fabrication of the oil-water interface in Fig. 2A.

The thickness of the oil layer can be varied by using different amount of oil. This thickness was estimated by moving the focal plane from the top surface of the glass substrate (which often contained scratches or stuck particles as markers) up to the oil-water interface where particles populated. The distance traveled by the focus was read from the focus knob. The thickness value obtained this way was supported by confocal microscopy shown in Fig. S1, and more precisely by a defocusing based algorithm (Fig. S2).[25]

To visualize the structure of the oil-water interface, 1 wt.% Rhodamine B was used to dye the aqueous phase, while 0.1 wt.% Nile Red was used to dye the silicone oil. The visualization of the overall view and approximate size of the oil-water interface was achieved through 3D scanning and reconstruction by laser confocal microscopy and Leica LAS X software, respectively. Examples are given in Fig. 1C and Fig. S1. The relative position of a fluorescent microsphere and an oil-water interface was also visualized in the same way, shown in Fig. S3.

A second type of oil-water interface used in Fig. S4 was constructed by adapting from ref. 26. First, two strips of double-sided adhesive tape with a thickness of 200 μm was affixed onto a hydrophobic glass slide. Then, a hydrophilic glass slide was placed on top of the adhesive tape. Between the two glass slides, 27 μL of oil was injected, followed by the careful injection of 3 μL water. This formed an oil-water interface, with the oil phase at the bottom and the water phase at the top. Upon loading the motors into the water phase, gravity caused the motors to settle near the oil-water interface. To compare motor speeds at both the oil-water interface and the glass substrate, the device was flipped so that water was at the bottom and oil at the top. Consequently, the motors settled on the hydrophilic glass substrate. This allowed for a direct comparison of the motor speeds between the oil-water interface and the glass substrate within the same experimental setup.

To study the effect on motor speeds by the chemicals that have possibly diffused from the oil to the water phase, the oil and water phases were allowed to contact for 12 hours, after which the water was collected and an appropriate amount of colloidal motors was dispersed in the "contaminated" water. Then, H_2O_2 was added to achieve an initial concentration of 5%, and the SiO_2-PtO motors in the contaminated water at the glass-water interface was observed.

The air-water interface was created by flipping the open chamber containing a drop of water on a hydrophilic substrate. Once flipped, the water remained in the chamber because of capillary forces, while motors in the water phase settled down to the air-water interface.

To modify the dissolved oxygen content in the water or oil phase of an oil-water interface, Ar, N_2, and O_2 were bubbled into deionized water or oil phase contained in serum bottles at a flow rate of approximately 3 mL/s for 2 hours. The treated water or oil phase was then used to create an oil-water interface, followed by the rapid execution of subsequent experiments. A gas-tight chamber was constructed by placing a clean cover slip on the top of the chamber, which was then sealed with UV-curable resin.

Motor Experiments. Different motors were activated by different energy sources. The fuel for PS-Pt, SiO_2-Pt, and SiO_2-PtO motors was 5% hydrogen peroxide (H_2O_2), and 0.5% H_2O_2 for SiO_2-Ag. For TiO_2-Pt, the fuel was water, 50 mM H_2Q or 500 μM TEOA. WO_3-Pt was fueled by 500 mM H_2Q, while SiO_2-AgCl moved in deionized water. Ultraviolet (UV) light was used to activate TiO_2-Pt, WO_3-Pt, and SiO_2-AgCl motors, with a light-emitting diode (LED) lamp (Thorlabs, M365LP1-C1) operating at 365 nm and 563 mW/cm^2. UV lighting was applied from above the microscope through Kohler illumination.

In a typical experiment, a setup of oil-water interface was placed next to a setup of glass-water interface above, both on the same sample stage of an inverted microscope. H_2O_2 was first added to the setup of oil-water interface, and videos were recorded typically within 30 s to 3 min afterward. Then, the same procedure was repeated in the setup of the glass-water interface, and the same amount of wait time and recording duration was used to ensure that the motor trajectories were obtained under comparable timescales for each case. Motor speeds typically decrease over time at either interface (Fig. S5).

Data Collection and Analysis. Videos were captured at a rate of 15-30 frames per second (fps). MATLAB was utilized to analyze the videos and extract the x-y coordinates of each motor, as well as their instantaneous velocities (codes curtesy of Professor Hepeng Zhang from Shanghai Jiaotong University). The tilt angle of the Janus motor was determined following ref. 27.

The Mean Squared Displacement (MSD) of each trajectory was calculated by:[28, 29]

$$\mathrm{MSD}(n\tau) = \frac{1}{N-n}\sum_{i=1}^{N-n}[(x_{(i+n)\tau} - x_{i\tau})^2 + (y_{(i+n)\tau} - y_{i\tau})^2] \quad (1)$$

where x and y are the centroid position of the particle, and nτ represents the time interval for calculating MSD, where τ is the acquisition time. To determine the 2D diffusion coefficient (D), the MSD curve was fitted by MSD(nτ)

$= 4D \cdot (n\tau)$. The videos used for MSD calculation were recorded at a frame rate of 30 frames per second. The value of τ is 0.033 seconds, and the range of n is 1 to 100. The total duration of Brownian motion for each particle that was statistically analyzed is 33.3 seconds, and the maximum value of $n\tau$ equals to 10% of the total duration of the entire motion trajectory. Before calculating MSD, a homemade MATLAB code was used to correct drift from the trajectories of the particles following ref. 30. The general principle of this method is to correct the instantaneous motion of each particle by subtracting the average of the vector of the particle's motion across the entire field of view.

The 3D trajectories of colloidal motor, particularly their instantaneous positions along the z-axis, were determined using a defocus-based algorithm (DefocusTracker) outlined in reference[25].[25] This method relies on the fact that for a fixed focal plane, a colloidal particle will exhibit different degrees of defocusing at different heights. In practice, a stack of images with varying degrees of defocusing were captured for a reference particle at various heights. To achieve this, the focusing knob of the microscope was manually adjusted to move the focal plane of the objective lens vertically while keeping the sample stage stationary. The algorithm then matched each image with its corresponding height. Subsequently, images captured during the actual experiment were compared to the reference stack to determine the height of 3D trajectories of the particle. The 3D speed of motors has been corrected for the settling speed due to gravity. A schematic of this procedure and a stack of reference micrographs are provided as Fig. S2.

Experiments Supporting the Reaction Acceleration at An Oil-Water Interface.

Growing Dendritic Silver Chloride (AgCl). Through slight modifications to a previous method,[31] dendritic silver chloride (AgCl) particles were grown by adding 6.7 μL of freshly prepared 14.3 mM $HAuCl_4$ and 0.5 μL of freshly prepared 10 mM $AgNO_3$ solution into an experimental chamber that contained either an oil-water interface or a glass-water interface. The growth of dendritic AgCl was observed and recorded by an inverted microscope.

The transformation of SiO_2-Ag Janus Particles in H_2O_2. SiO_2-Ag Janus particles were added to the experimental chamber, followed by the addition of H_2O_2 to achieve a final concentration of 1.5%. The time it took for the dark Ag coating to be oxidized by H_2O_2 was monitored under the inverted microscope.

Measurement of H_2O_2 consumption. The measurement described below follows those given in ref. 32 and the manual from the assay kit vendor. 5 μL of deionized water containing 5 μm PS-Pt or SiO_2-Pt Janus motors was added to both chambers containing each interface with 2D population density (ϕ) between 3% and 4% (determined by the packing fraction of motors on a 2D plane they resided on using ImageJ). Then, 5 μL of 10% H_2O_2 was added to both interfaces simultaneously, making the initial concentration of H_2O_2 5% and initial reaction volume 10 μL. After 10 minutes of reaction, the water in each chamber was carefully collected by a 20 μL pipette tip. The obtained H_2O_2 aqueous solution was transferred to 1.5 mL centrifuge tubes, diluted to 100 μL, and centrifuged twice (2000 rpm, 1 min) to remove colloidal particles. Then, 75 μL of the supernatant was taken, diluted with deionized water to 100 μL, and mixed with 1 mL of reagent 1 (buffer solution) and 1 mL of reagent 2 (ammonium molybdate reagent) from the hydrogen peroxide assay kit.

H_2O_2 reacts with ammonium molybdate to yield a stable yellow complex. The optical density (OD) of this complex at 405 nm is linearly related with the concentration of H_2O_2 in the range of 1.5 mM to 150 mM. The OD value was obtained by UV-Vis spectroscopy at 405 nm (scanned between 300 - 500 nm at a rate of 1.67 nm s^{-1}). A calibration curve was provided by the producer of the assay kit, given in Fig. S6. The reaction rate constant k at either an oil-water interface or a glass-water interface at t=10 min was then calculated by $k=\ln(A_0/A_{10min})$, where A_0 is the OD of the unreacted 5% H_2O_2 solution (after dilution as described above), and A_{10min} is that of the collected H_2O_2 solution after reaction from that interface.

Calculation of the enhanced interfacial transport. Following ref. 33, the interfacial transport is enhanced by 1+b/L, where b is the slip length and *L* is a measure of the interfacial thickness. In our experiments, all motors are believed to operate under a self-generated electric field, so that L is comparable to the Debye length,[33] estimated to be ~ 7 nm in 5 wt.% H2O2 of an electrical conductivity of 1.2×10^{-6} S/cm.[34] This conductivity is close to the conductivity of a 2 mM KCl solution measured in our laboratory (0.93×10^{-6} S/cm). Assuming these two solutions have the same ionic strength, the Debye length λ of 5 wt.% H2O2 is determined to be ~7 nm. Using the same b=30 nm as in ref. [33], the 1+b/L scaling then predicts a speed increase of V/V=1+b/L=5.2.

RESULTS

Micromotor speeds increase at an oil-water interface. In a typical experiment, an oil-water interface was constructed by placing 8 μL water droplet containing micromotors and fuel molecules on a thin film of silicone oil spread on a hydrophobic glass slide (Fig. 1C, see Experimental section for details). This results in an oil-water interface with water above a thin layer of oil of a few μms thick (see Experimental details for measurement of thickness). Thicker oil layers up to ~200 μm do not qualitatively change the results described below (Fig. S7). Nor does whether the chamber is open or sealed from the top. Micromotors settled from the water phase to the oil-water interface. Below, we will show that they reside slightly above the interface, rather than becoming trapped in the interface. Because of gravity, the water droplet formed a lens shape that is thicker at the center than its edge (Fig. S1). In the absence of chemical fuels, colloids over 30 min to 1 h were gradually collected to the center of the bottom of the water lens. However, this effect was negligible for chemically powered motors, so a flat interface is assumed

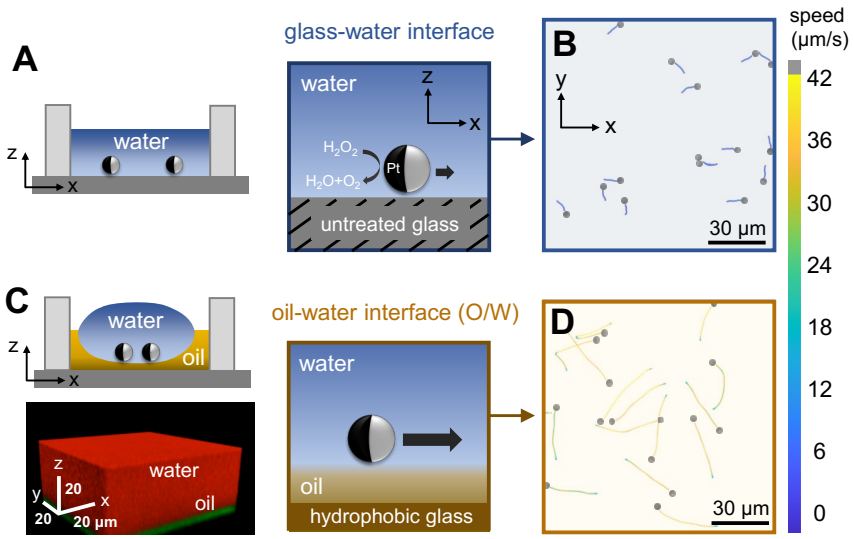

Figure 1. Micromotor moving on glass-water (top) and oil-water (bottom) interfaces. (A, C) schematics of the experimental setup for motor experiments on a glass-water interface (A) or an oil-water interface (C). The zoomed-in confocal micrograph of a section of the oil-water interface is shown in (C), and Fig. S1 contains a micrograph at a smaller magnification. (B, D) Trajectories over 2 s and instantaneous speeds (color coded) of 3 μm polystyrene-platinum (PS-Pt) Janus micromotors in 5 wt.% H_2O_2 on a glass substrate (B) and on a silicone oil-water interface (D). Results in B and D are taken from Movie S1.

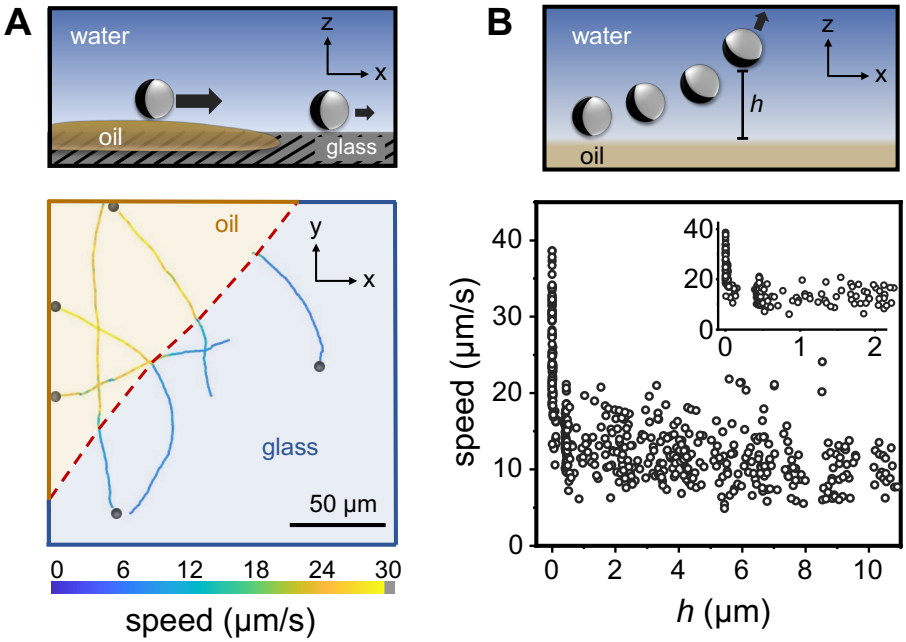

Figure 2. Evidence of the speed increase of micromotors at oil-water interfaces. (A) Schematic (top) and actual trajectories (bottom) of the acceleration of 5 μm PS-Pt micromotors when moving from the surface of a glass substrate to a silicone oil-water interface. A dashed line is hand-drawn to indicate the boundary of the thin oil droplet. Instantaneous motor speeds are color-coded. Results are taken from Movie S2. (B) Schematic (top) and instantaneous motor speeds (bottom) of 5 μm PS-Pt micromotors moving from a silicone oil-water interface to the bulk fluid. It moves upward likely because of a heavier Pt cap that oriented toward its bottom, similar to ref. 35. Inset: data in the range of h=0-2 μm. Results are taken from Movie S3. The height h is defined in the top schematic, and experimentally determined by a defocusing tracking algorithm detailed in Experimental sectiat and adapted from ref. 25. All experiments were performed in 5% H_2O_2. Data in B were acquired from 5 motors tracked in 5 separate experiments.

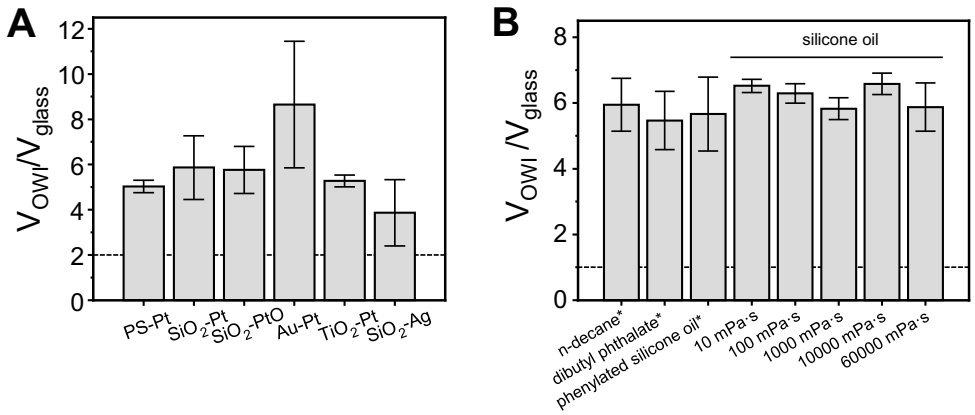

Figure 3. The increase of motor speeds at oil-water interfaces for different types of motors (A) and at interfaces made of different oils (B). $V_{o/w}$ and V_{glass} is the motor speeds at an oil -water interface and on the surface of a glass substrate, respectively. The last 5 set of data in (B) were acquired from interfaces made with silicon oil of different viscosities and from PS-Pt motors. SiO_2-PtO motors, however, were used in experiments with oils marked with * because PS dissolves in them. Error bars represent one standard deviation of over 200 individual micromotors moving for at least 10 s. See the main text for a description of different types of motors in (A), and see the Experimental section for their synthesis.

throughout this article. Experiments below were typically performed with polystyrene (PS) or silicon dioxide (SiO_2) microspheres, of 3 or 5 μm diameter and half-coated with 20 nm platinum (Pt) (See Fig. S8 for the scanning electron micrographs). In hydrogen peroxide (H_2O_2) aqueous solutions of typically 5 wt.%, these PS-Pt or SiO_2-Pt Janus microspheres moved away from their Pt caps where H_2O_2 catalytically decomposed into H_2O and O_2 (Fig. 1A).[36, 37] These Pt Janus motors are archetypical chemical micromotors widely used as model systems.[38] However, other types of chemical micromotors and oils were also tested and results are detailed below.

Remarkably, these Pt Janus motors moved at an oil-water interface significantly faster than those moving on a glass-water interface under otherwise identical experimental conditions. For example, Fig. 1B and 1D and Movie S1 show that the average speed of 3 μm PS-Pt micromotors was 36.0 ± 5.4 μm/s (± refers to one standard deviation) on a silicone oil-water interface, versus 7.3 ± 1.5 μm/s on a common glass slide. The speed ratio, denoted throughout in this article as $V_{O/W}/V_{glass}$ or simply V/V, is ~5. A speed increase of 4-6 fold was also found for PS-Pt motors of sizes ranging from 1-10 μm in diameter (Fig. S5). We also confirm in Movie S4 that drift at or near the oil-water interface, or in the bulk water, was small and did not cause the speed increase we report here.

To further confirm the speed increase, motor speeds at an oil-water interface were compared *in situ* with those on a glass substrate, by using a setup that contained both an oil-water interface and a glass-water interface *side by side* (Fig. 2A, see Experimental section for fabrication details). In this setup, 5 μm PS-Pt micromotors moved in 5% H_2O_2 at 6.9 $\pm$ 1.3 μm/s on a glass substrate, but immediately accelerated to 22.7 $\pm$ 1.7 μm/s when they moved on the surface of a thin patch of oil.

Moreover, the speed increase was limited to the close vicinity of an oil-water interface. For example, Fig. 2B shows that the speeds of 5 μm PS-Pt micromotors drastically reduced from 30-40 μm/s to ~10 μm/s in 5% H_2O_2 when they moved only 1 μm upward and away from the oil-water interface, and further reduced to ~ 8 μm/s when they reached the bulk fluid (obtained by 3D optical tracking, see Experimental section for details).

The speed increase of micromotors at an oil-water interface is a robust effect found for a variety of chemical micromotors, powered by pure water or H_2O_2, and at interfaces made with different types of oils. For example, Fig. 3A and Movie S5 demonstrate such acceleration of spherical micromotors made of PS-Pt, SiO_2-Pt, SiO_2-PtO, Au-Pt, TiO_2-Pt, and SiO_2-Ag. Among them, PS-Pt, SiO_2-Pt and SiO_2-PtO[18] micromotors move by decomposing H_2O_2 on their Pt (or PtO) caps, likely via self-electrophoresis.[23, 39]Au-Pt microspheres decomposed H_2O_2 on both caps,[39, 40] and TiO_2-Pt motors moved in water under UV light, both via self-electrophoresis.[41] SiO_2-Ag motors moved in H_2O_2 via ionic self-diffusiophoresis.[41-44] Despite their differences in materials, fuels and propulsion mechanisms, all motors tested here were chemically powered and moved in self-generated electric fields. They all moved faster at an oil-water interface than on a glass substrate, with speed ratios ranging from 5 to 8. Au-Pt microsphere motors showed the highest V/V of ~8. In addition, Fig. 3B and Movie S6 show that the choice of oil had minimal effect on the speed increase, as Pt motors moved at similar speeds at an oil-water interface made of decane, dibutyl phthalate, phenylated silicone oil, silicone oils of different viscosities, or fluorinated oils, despite their differences in chemical composition and physical properties (see Table S1 for details).

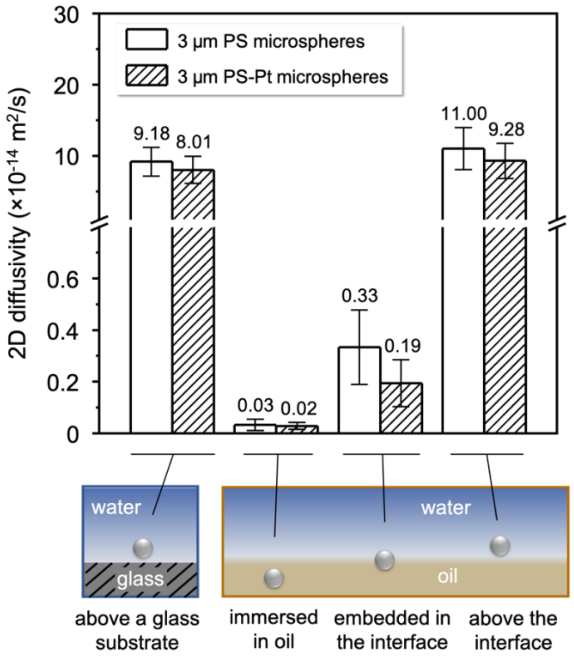

Figure 4. 2D diffusivities of 3 μm PS or PS-Pt microspheres in four scenarios as illustrated in the bottom panels. Deionized water of 18.2 MΩ is used in all cases, except for the second scenario, where 10 mM KCl aqueous solution was used to force particles into the interface. Silicone oils of a viscosity of 1000 mPa·s were used. The diffusivity values were obtained from the mean squared displacement (MSD) of the Brownian motion of the microspheres in each scenario (see Fig. S10, S11 and Movie S7 for the original data).

Micromotors are slightly above the oil-water interface. Naively, a micromotor could be hovering above an oil-water interface in the water phase, embedded in the interface, or immersed in the oil phase (Fig. 4). However, the following pieces of evidence strongly suggest that a micromotor is situated slightly above the oil-water interface. First, since both the PS or SiO_2 particles (zeta potential = -50.6 ± 0.2 mV and -40.5 ± 2.7 mV, respectively) and oil droplets suspended in water (-25.0 ± 0.7 to -36 ± 1.2 mV for different oils, see Fig. S9) carried negative charges, a motor would be electrostatically repelled by the oil-water interface when settling from above. Second, tracer microspheres behave qualitatively the same around a micromotor moving either on a solid substrate or at an oil-water interface (Movie S4). Nor do two micromotors interact with each other in qualitatively different way on these two interfaces (MoiveS1). Third, Fig. 4 shows that the 2D diffusivity of a PS microsphere located at an oil-water interface is closest to the one settled to a glass surface, but much higher than the diffusivity of a PS microsphere either immersed entirely in oil, or trapped in an oil-water interface (see Experimental section for details and Fig. S10 for mean squared displacement results). PS-Pt Janus microspheres of zeta potential of -61.5 mV behaved qualitatively the same (Fig. S11). A previous study[45] has used the same measurement of diffusivity to show that negatively charged particles tended to remain in water above an oil-water interface, unless chemicals such as surfactants or alcohols were added to overcome the interfacial energy barrier. Last but not the least, confocal microscopy provided direct visualization of a fluorescent microsphere situated slightly above an oil-water interface (Fig. S3).

Faster chemical reactions power faster micromotors at an oil-water interface. We propose that chemical reactions that power a micromotor occur faster at an oil-water interface, resulting higher motor speeds (Fig. 5A). This mechanism is inspired by previous reports that show faster reactions on the surface of water droplets,[46-50] presumably because of the charges accumulated at the oil-water or air-water interface.[47, 48, 51] More relevant to the current discussion, an earlier study[41] has found that hydrophobic micromotors were about twice as fast as their hydrophilic counterparts in H_2O_2. This speed increase was speculated to arise from faster decomposition of H_2O_2 on the hydrophobic surface of a hydrophobic motor than the hydrophilic one. It is therefore reasonable to suspect that the reactions powering our micromotors occur faster on top of hydrophobic oils.

Two experiments indirectly support this hypothesis that faster reactions at an oil-water interface drive micromotors faster. First, Fig. S12 shows that AgCl dendrites, formed by the reaction of $AgNO_3$ in $HAuCl_4$ aqueous solutions, grew substantially larger on a silicone oil -water interface than those grown above a glass substrate. Second, Fig. S13 shows that the Ag caps of SiO_2-Ag Janus microspheres dissolved in H_2O_2 substantially faster on a silicone oil-water interface than those on a glass substrate. Although neither chemical reaction powers our micromotors, these two results suggest that some chemical reactions indeed occur faster on the same oil-water interface as used in our motor experiments.

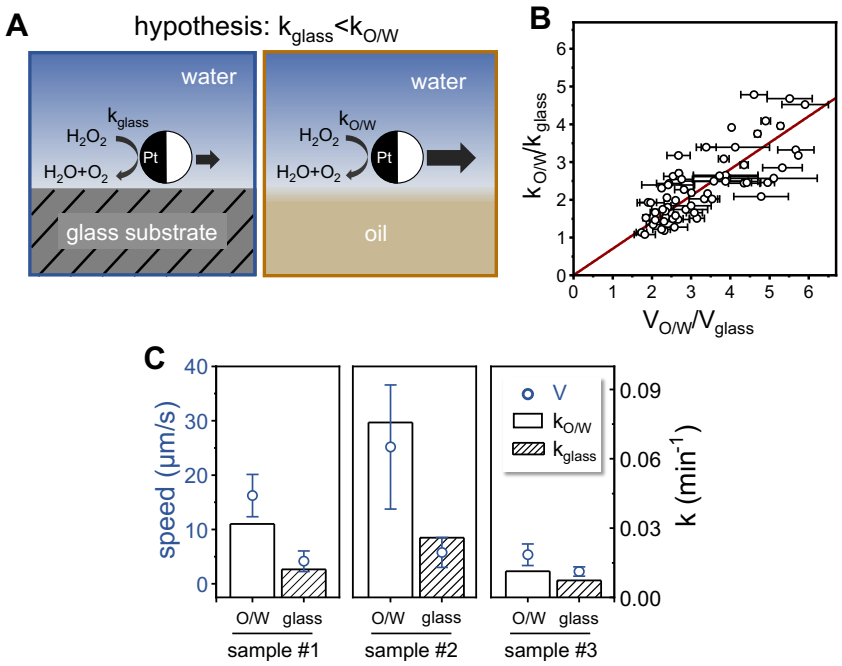

Figure 5. Fast motor propulsion at an oil-water interface due to fast reactions. (A) Schematic showing that a Pt micromotor catalyzes the decomposition of H_2O_2 faster at an oil-water interface, with a rate constant $k_{O/W}>k_{glass}$. (B) Plotting $k_{O/W}/k_{glass}$ against their speed ratios $V_{O/W}/V_{glass}$, obtained from multiple measurements of Pt Janus micromotors moving in H_2O_2. Red solid line: linear fit of all data points through origin, with $R^2 = 0.94$. (C) Representative data of reaction rate constants k (bar plots, right axis) and motor speeds V (circles, left axis) at an oil-water interface and on a glass substrate from three sets of experiments. Note how higher k always corresponds to higher V, and how the ratio of k/k and V/V is similar in each set of experiments. All error bars represent the standard deviation from over 200 motors. 5 μm Pt Janus micromotors, 5% H_2O_2 and silicone oil of 1000 mPa·s were used.

We confirm that the catalytic decomposition of H_2O_2, the reaction powering many of our micromotors, indeed occurs faster at an oil-water interface than near a glass substrate. To elaborate, we measured the reaction rate of the catalytic decomposition of H_2O_2 by PS-Pt motors on a silicone oil-water interface, and compared it with that on a glass substrate. To do so, the H_2O_2 concentration in the water phase (above either an oil layer or a piece of glass) at the beginning of the experiment and at t=t was determined respectively by colorimetry (see Experimental sectiat and Fig. S6 for details) as c_o and c_t. The reaction rate constant k was determined assuming a first order reaction kinetics by $c_t=c_o\exp(-kt)$, where t is the elapsed time. Since experiments on either an oil-water interface or a glass-water interface were performed with the same H_2O_2 concentration, the term "reaction rate" will be used interchangeably below with "reaction rate constants" when describing the rate of reactions.

Importantly, the results in Fig. 5B and 5C show that not only are the reaction rates at oil-water interfaces consistently larger than those obtained on a glass substrate, their ratio ($k_{O/W}/k_{glass}$) also correlates positively with the ratio of the motor speeds ($V_{O/W}/V_{glass}$). Three sets of experiments of different motor speeds and reaction rates are listed in Fig, 5C as examples. Taken together, the observations of faster decomposition of H_2O_2, faster AgCl growth and faster Ag dissolution at an oil-water interface collectively suggest that chemical reactions proceed faster at an oil-water interface, thus powering a micromotor to move faster, than on a glass substrate.

Why do H_2O_2 decompose faster at an oil-water interface? We initially hypothesized that, because both oil and O_2 are nonpolar, O_2 dissolves in oil much more easily than in water, thus removing the product of the decomposition of H_2O_2 from water and accelerating the reaction as a result. Alternatively, ref. 52 proposed that O_2 is transported more effectively by a water depletion layer near hydrophobic surfaces, increasing the reaction rate of H_2O_2 decomposition. Both hypotheses are in seeming agreement with an earlier study[53] that had proposed that lowering the O_2 concentration in water significantly caused Au-Pt nanomotors to move faster in H_2O_2. However, our own experiments in Fig. S14 showed that PS-Pt motors moved at similar speeds in water containing different concentrations of O_2, prepared by saturating water with O_2, Ar or N_2 (in gas-tight chambers). Moreover, Fig. S15 shows that motors moved at similar speeds above an oil-water interface prepared with either untreated silicone oils, O_2-saturated silicone oils, or fluorinated oils (of high O_2 solubility). These results disapprove the hypothesis that O_2 dissolution in oil accelerates the chemical reactions at an oil-water interface. An alternative hypothesis is yet to be found.

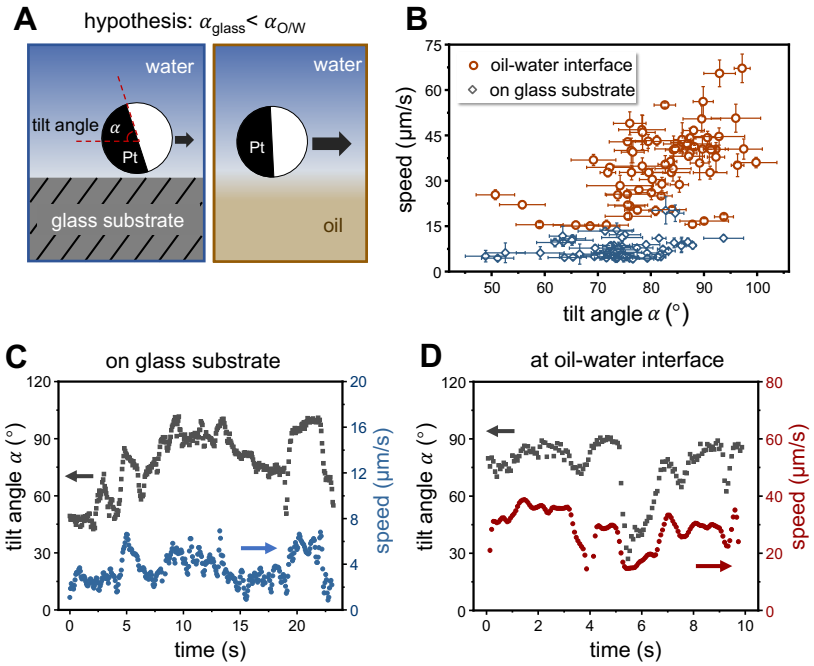

Figure 6. Tilt angles of a Janus motor on an interface. (A) Schematic showing the hypothesis that a Janus microsphere motor moves with a larger tile angle (α, defined in the left panel) at an oil-water interface than on a glass substrate. The Janus particle is assumed to move with its heavy Pt hemisphere tilted downward. (B) Speeds and tilt angles of micromotors moving at an oil-water interface (orange empty circles) and on a glass substrate (grey empty diamonds). Each circle in (B) represents one micromotor. Errors are standard deviation of 200 data points averaged over 10 s. (C and D) Tilt angles (left y axes) and motor instantaneous speeds (right y axes) of one representative PS-Ni-Pt motor on a glass substrate (C) or at an oil-water interface (D), respectively. The instantaneous tilt angle of the motor was adjusted *in situ* by a hand-held magnet, and its speeds varied accordingly. Note that the highest speeds on a glass substrate are still a few times smaller than the lowest speeds at an oil-water interface. 5 μm PS-Pt microspheres, 5% H_2O_2 and silicone oil of 1000 mPa·s were used unless otherwise specified.

DISCUSSION

We now discuss a few additional possibilities for the speed enhancement of motors at an oil-water interface. We then detail tips/caveats for observing an increase in motor speeds at oil-water interfaces, which could be important for determining its mechanism. Finally, we discuss how our results compare with previous reports of chemical micromotors moving on/near oil-water interfaces.

Speed enhancement is not caused by larger tilt angles at an oil-water interface. A tilt angle is defined as the angle between the plane separating the two caps of a Janus motor and the substrate it moves on, through the Pt hemisphere (Fig. 6A). For a chemical micromotor near a boundary, this angle arises from a complicated interplay among the wettability and density distribution of the motor, the electrostatic properties of both the motor and the interface, and localized distributions of chemicals, electric fields and fluid flows.[54-57] We discovered earlier[27] that the closer the tilt angle of a motor is to 90°, the faster it moves, likely because only a fraction of the propulsive force is aligned with the moving direction for a tilt angle other than 90°. Here, we found that (Fig. 6B) PS-Pt micromotors moved with tilt angles closer to 90°at an oil-water interface than those moving on a glass substrate, echoing ref. 17. This correlation, however, does not suggest that larger tilt angles *caused* higher motor speeds at an oil-water interface. To elaborate, we have manually changed the tilt angles between ~30°-90° of magnetic 5 μm PS-Ni-Pt Janus micromotors. Results in Fig. 6C and 6D show that even though motor speeds can be modulated by magnetically tilting it, a motor on a glass substrate never moved as fast as a motor at an oil-water interface, and a motor at an oil-water interface never slowed down to the same level as a motor on a glass substrate. These results suggest that motors move *inherently* faster at an oil-water interface than on a glass substrate, which could cause a larger tilt angle, but not the other way around.

Hydrodynamic slips cannot explain speed enhancement. Results from an earlier study[58] suggested that Pt Janus motors moved faster on hydrophobic substrates than hydrophilic ones in H_2O_2, possibly because of an enhanced interfacial transport by the higher hydrodynamic slips on hydrophobic surfaces.[33] More quantitatively, ref. 48 proposed that $V \propto (1+\cos\theta)^{-3/2}$, where V is the motor speed and θ is the contact angle of water on the substrate. This scaling predicts that motors move on a hydrophobic substrate of θ = 140° (a reasonable value of an oil-water interface from ref. 59) 22.8 times faster than motors moving on glass of θ = 20°. Alternatively, ref. 33 proposed that the amplification of interfacial transport scales with $1+b/L$, where b is the slip length and L is a measure of the interfacial thickness. This scaling then predicts a 5.2

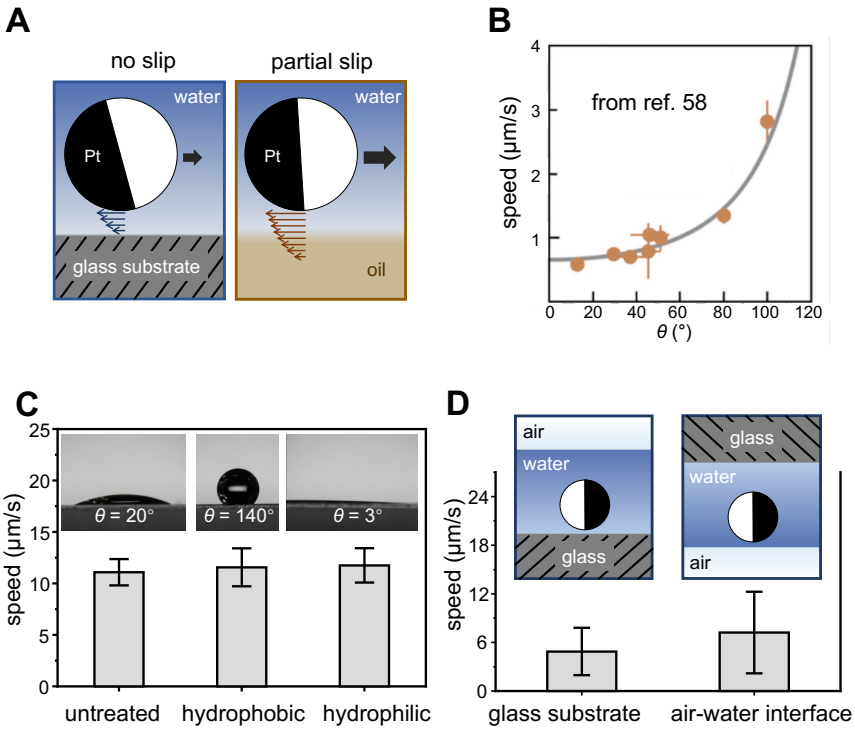

Figure 7. The effect of interfacial slips on the speeds of chemical motors. (A) Schematic showing that a glass substrate has a smaller hydrodynamic slip than that at an oil-water interface, so that a chemical micromotor might move more slowly on the former than the latter interface. (B) speeds of motors moving on substrates with various contact angles with water, reported in ref. 58. Figure adapted with permission under a Creative Commons Attribution 4.0 International license from ref. 58. Copyright American Physical Society 2020. (C) Motor speeds on three glass slides of different water contact angles (inset). (D) Motor speeds on a regular glass substrate or on an air-water interface, which was obtained by flipping the setup upside down. PS-Pt microspheres of 3 (C) or 5 (D) μm in diameters and 5% H_2O_2 were used.

fold speed increase for motors moving at an oil-water interface (see Experimental section for calculations). Both scaling are qualitatively in agreement with our observed speed increase of 4-6 fold. Both scaling also predict that motors move at very different speeds on glass substrate of $\theta = 140°$, 20°, or 3°, and at an air-water interface that is completely slippery. However, Fig. 7C shows that chemical motors moved at similar speeds on these interfaces. Therefore, although theoretically plausible, speed enhancement by a slippery surface cannot explain the observed speed enhancement of motors at oil-water interfaces.

Speed enhancement is not caused by interfacial electroosmosis. Electroosmosis refers to the flow of charged fluid layer near a charged surface in a tangential electric field. It has been suggested earlier[60, 61] that micromotors are slowed down near a negatively char[61]ged solid surface because the electroosmotic flow advects the motor in the opposite direction to its propulsion. It is possible that such an adverse electroosmotic flow is weaker at an oil-water interface, because it carries a less negative surface charge (~ -30 mV, see Fig. S9) than a typical glass substrate (-68.0 mV or -72.9 mV[62]). As a result, a micromotor would move faster (or *slowed down less*) at an oil-water interface than a glass substrate. This line of reasoning predicts that a motor moves faster in the bulk solution than one moving near either an oil-water interface or a glass substrate, because electroosmosis, and consequently the reduction in motor speed it causes, vanishes in the bulk fluid. This prediction is, however, contradictory to our measurement in Fig. 2B, and suggests that the interfacial electroosmosis is not a dominant factor in enhancing motor speeds at an oil-water interface.

Speed enhancement is not caused by chemicals leaching from oils into water. It is also possible that certain chemicals diffused from oil into water and accelerated motors. Without identifying the exact identity or effect of such chemical species, we disapprove this hypothesis in Fig. 8A by showing that motors do not move at an enhanced speeds in the "contaminated" water that was in contact with an oil. Fig. 3 also shows that the extent of speed increase was similar for an oil-water interface made with dibutyl phthalate, which was partially soluble in water, with interfaces made of insoluble oils such as n-decane and silicone oil. These results collectively suggest that chemicals diffusing from the oil phase into the water phase, if any, had a negligible effect on motor speeds.

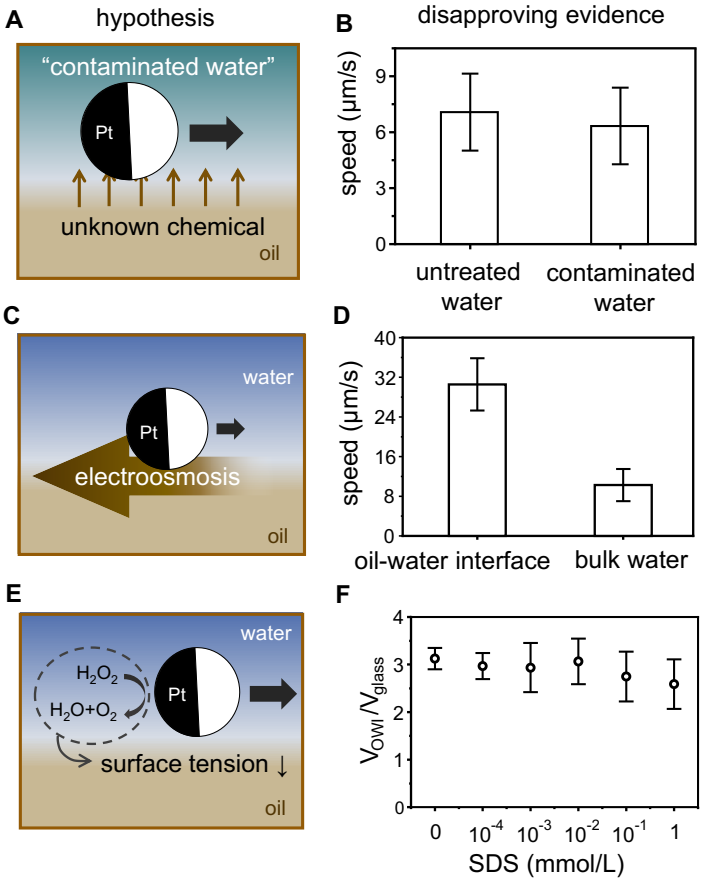

Figure 8. Three additional hypotheses (A, C and E) to explain the enhanced motor speeds at oil-water interfaces and key evidence (B, D, and F) that disapprove these hypotheses. (A, B) chemicals are suspected to diffuse from the oil phase into water, accelerating motors, but their speeds (B) were similar in regular water or in water collected above an oil. (C, D) it is suspected that electroosmosis that slows down a motor is weaker at an oil-water interface than on a glass substrate, but motors move a few times faster on an oil-water interface than in the bulk water (D, data taken from Fig. 2B), opposite to what this hypothesis predicts. (E, F) It is suspected that chemicals resulting from catalysis on the motor surface reduces the local surface tension, so that Marangoni flows provide additional propulsion to the motor, but interfaces with various amount of surfactant (sodium dodecyl sulfate, SDS) lead to speed enhancements of similar magnitudes (F). 5% H_2O_2 and silicone oil of 1000 mPa·s were used. Motors were 5 μm SiO_2-Pt microspheres in B, 5 μm PS-Pt in (D), and 3 μm PS-Pt in (F).

Speed enhancement is not caused by a change in interfacial surface tension. Surface tension gradients are long known to cause microscopic objects to move on liquid-liquid or liquid-air interfaces, such as the classical examples of camphor boats.[63] This effect could also be present in our experiment, as the chemical motors near the interface consume and produce chemicals that could create gradients in surface tension along the oil-water interface. However, this hypothesis is disapproved by two pieces of evidence. First, the interfacial tension and the flows caused by interfacial tension gradient is greatly affected by the presence of surfactants,[64] yet Fig. 8E shows that motors moved at similar speeds at oil-water interfaces when different concentrations of surfactants (either ionic or non-ionic, Fig. S16) were added in water (note that motors still remained above the interface after the addition of surfactants). Second, objects surfing in surface tension gradients interact strongly with each other in the form of attraction, repulsion, self-assembly and even synchronization.[63] However, Movie S1 shows none of these interactions among motors or between a motor and a tracer at oil-water interfaces beyond what is typically seen on a regular glass substrate. In addition, as described earlier, we do not see any significant drift indicating Marangoni flows. Nor do we see collective migration of many motors in the same direction as dictated by drifting.

Experiment details for observing the increase in motor speeds at oil-water interfaces. To help readers reproduce our results, we provide the following technical details critical for successfully observing the speed increase of micromotors at an oil-water interface. Much of these experimental caveats remain poorly understood.

a. Successful hydrophobic modification of the glass substrate is important to ensure the stability of the oil-water interface. Otherwise, the interface could collapse within minutes or seconds and motors (with the water phase) fall to the surface of underlying glass substrate, where they resume their "typical" speeds.

b. Equally important is the "freshness" of the motors, as they often exhibited the highest speed increase when tested immediately after they were fabricated. For example, the speed ratio of $V_{O/W}/V_{glass}$ decreased from 4.7 to 2.2 when 3 μm PS-Pt motors were shelved for 1 month. We recommend storing the sample (after physical deposition but before being released from the substrate) in a sealed bag under vacuum.

c. The speed increase of a chemical micromotor at an oil-water interface is a *common but not universal* effect. Specifically, speed increase was more consistently found for PS-Pt and SiO_2-PtO motors than SiO_2-Pt motors. Moreover, data in Fig. 3A show that the speed increase is significantly more pronounced for Au-Pt microspheres (V/V=8) and PtO Janus microspheres (V/V=6.1), both moving in H_2O_2, than the other types of motors we have tested. Furthermore, the speed increase of photochemical TiO_2-Pt motors is significantly stronger in water (V/V=5.0) than in hydroquinone (V/V=1.7) or triethylamine (V/V=2.5), despite that the latter two are both effective fuels that power motors in high speeds on a glass substrate.[65, 66] Nor do WO_3-Pt motors[17] in hydroquinone move significantly faster at an oil-water interface (V/V=1.6). SiO_2-AgCl motors[24] in water even moved more slowly at an oil-water interface, with a V/V =0.9. These results of weak (or no) speed increase are shown in Fig. S17 and Movie S8. We do not understand the differences in the degree of speed increase among different types of motors or fuels. We also suspect (from empirical evidence) that a trace amount of Au during the deposition of Pt could significantly increase the motor speeds moving on both interfaces, and lead to a large speed enhancement.

d. We have consistently observed higher speed increase when the oil-water interface was constructed in the method reported above instead of the method used in ref. 26, where the water and oil layer is sandwiched between a top hydrophilic and a bottom hydrophobic glass substrate (see Fig. S4 for schematics and Fig. S18 for motor speeds).

e. Although an increase in motor speed at an oil-water interface is a qualitatively robust observation, the exact magnitude of the increase, or the absolute speeds, varies from one experiment to another, even under identical experimental conditions with the same samples. This inconsistency, seen as large error bars in all the speed ratios reported in this study, possibly reflects the complexity associated with this phenomenon. To improve consistency, the experiment at an oil-water interface was performed immediately after the experiment on a glass substrate, and a new sample of motors were taken from the same vial for each experiment.

Note that motors prepared in different batches or tested in different conditions often move in significantly different speeds. Therefore, speed ratios (V/V) are used throughout this article, because it is often the speed ratio, rather than the absolute speeds (given in Fig. S19), that carries the significance this study.

Comparison between our results with previous reports of micromotors at oil-water interfaces. Two previous studies have reported the speeds of chemical micromotors (Pt Janus motors as used here) moving on/near oil-water interfaces. Specifically, SiO_2-Pt motors in ref. 18 moved consistently more slowly along a vertical oil-water interface near an oil droplet than those moving on a glass substrate. However, the configuration of this oil-water interface is significantly different from the flat interface used in our study, so that motor speeds are not only affected by the oil-water interface but also by the glass substrate underneath. In addition, the motor in ref. 67 is trapped in a wedge, which could significantly affect its speed in its own way (e.g. confinement[68]). To summarize, a motor moving next to oil droplets as in ref. 18 could be affected by physico-chemical mechanisms beyond those dominating on a flat oil-water interface.

On the other hand, ref. 19 reported that motors on the surface of an oil patch moved at similar speeds to those on a glass substrate. This experimental setup is very similar to ours in Fig. 2A, and in principle should result in significant enhancement in motor speeds. We repeated the experiments from ref. 19 with experimental conditions as close to ref. 19 as possible, so that motors moved in a sealed chamber, on fluorinated oil, and in the presence of 0.0025 wt% specialized fluorosurfactant. However, unlike ref. 19, we saw ~3-fold speed enhancement of motor speeds moving on such oil patches (36.3 ± 11.1 μm/s vs 12.3 ± 4.5 μm/s). To explain the difference, we speculate that the samples used in ref. 19 were in a different condition than ours, as we emphasized above, so that speed enhancement was not significant (in fact, a slight speed increasement can be inferred from the data in ref. 19, but not as much as ours).

CONCLUSION

In conclusion, we have reported that chemical micromotors move significantly faster at an oil-water interface than those moving on a glass substrate. The speed increase was typically 3-6 fold, but could be more than 10 fold in some cases. This significant increase in motor speeds occurs only in the close vicinity to an oil-water interface, and was observed for a variety of chemically powered micromotors, in pure water or H_2O_2, and at interfaces made with different types of oils. Evidences strongly suggest that micromotors are situated slightly above the interface in the water phase. There, chemical reactions occur faster than they would be on a glass substrate, which could power micromotors into faster propulsion. Other factors, such as tilt angles, hydrodynamic slops, interfacial permeability, electroosmosis, and surface tension gradients, were found to play small or

no roles in the observed speed increase. Open questions remain, such as the exact mechanism for fast chemical reactions at an oil-water interface, or how motor types of conditions affect their speed enhancement.

Our observation of the significant speed increase of chemical motors at oil-water interfaces provides valuable insights into the complex interactions between micromotors and their environments. Looking forward, this discovery could have important practical implications for applications of micromotors involving liquid-liquid or air-liquid interfaces, such as human bodies, oil recovery, food processing, etc., and for designing micromotors of high performance and energy efficiency.[12, 43, 61, 69-71] In addition, the speed increase effect is extremely sensitive to how far a motor is away from an interface (see Fig. 2B), and this feature can be potentially leveraged to design microsensors of an oil-water interface of exceptional sensitivity. Finally, the possibility that motors are powered by chemical reactions that are faster at an oil-water interface suggests that chemical micromotors could be used as a visible probe for real-time and quantitative measurements of the reaction rates at an oil-water interface.

ASSOCIATED CONTENT

Supporting Information.

The supporting information is available free of charge via the Internet at http://pubs.acs.org.

Supplementary Figures S1-S19 and Table S1.

Movie S1, PS-Pt micromotors moving on a glass substrate or at an oil-water interface.

Movie S2, PS-Pt micromotors moving across a substrate that contains both a glass-water interface and an oil-water interface.

Movie S3, PS-Pt micromotor moving away from an oil-water interface.

Movie S4, tracer microspheres around micromotors moving on a solid substrate or at an oil-water interface.

Movie S5, Speeds of five types of chemical motors on a glass substrate or at an oil-water interface.

Movie S6, Micromotors moving at an oil-water interface made with different oils.

Movie S7, the Brownian motion of 3 μm PS microspheres in different positions relative to an oil-water interface or above a glass substrate.

Movie S8, Various light-powered micromotors on a glass substrate or at an oil-water interface.

AUTHOR INFORMATION

Corresponding Author

Wei Wang – School of Materials Science and Engineering, Harbin Institute of Technology (Shenzhen), Shenzhen, Guangdong 518055, China; orcid.org/0000-0003-41633173; Email: weiwangsz@hit.edu.cn

Authors

Jiayu Liu – School of Materials Science and Engineering, Harbin Institute of Technology (Shenzhen), Shenzhen, China, 518055

Zhou Yang – School of Materials Science and Engineering, Harbin Institute of Technology (Shenzhen), Shenzhen, China, 518055

Zuyao Yan – School of Materials Science and Engineering, Harbin Institute of Technology (Shenzhen), Shenzhen, China, 518055

Shifang Duan – School of Materials Science and Engineering, Harbin Institute of Technology (Shenzhen), Shenzhen, China, 518055

Xiaowen Chen – School of Materials Science and Engineering, Harbin Institute of Technology (Shenzhen), Shenzhen, China, 518055

Donghao Cui – School of Materials Science and Engineering, Harbin Institute of Technology (Shenzhen), Shenzhen, China, 518055

Dezhou Cao – School of Materials Science and Engineering, Harbin Institute of Technology (Shenzhen), Shenzhen, China, 518055

Ting Kuang – Education Center of Experiments and Innovations, Harbin Institute of Technology (Shenzhen), Shenzhen, China, 518055

Xing Ma – School of Materials Science and Engineering, Harbin Institute of Technology (Shenzhen), Shenzhen, China, 518055; Sauvage Laboratory for Smart Materials, Harbin Institute of Technology (Shenzhen), Shenzhen, China, 518055

ACKNOWLEDGMENT

This project is financially supported by the National Natural Science Foundation of China (T2322006) and Shenzhen Science and Technology Program (RCYX20210609103122038, JCYJ20210324121408022). We thank Yong Wang, Xiaoxia Liu, Liying Wang from the Ma lab for the assistance with UV-Vis spectrophotometer, zeta potential analyzer, and contact angle goniometer. We also thank Zhaoyang Zhang and Prof. Ji Li for the assistance with dissolved oxygen meter. We also thank Xianglong Lyu, Qiang Gao, Ruitong Zhu, Xianghong Liu from the Wang lab for their assistance.

REFERENCES

(1) Hu, C.; Pané, S.; Nelson, B. J. Soft Micro- and Nanorobotics. Annual Review of Control, Robotics, and Autonomous Systems 2018, 1 (1), 53-75. DOI: 10.1146/annurev-control-060117-104947 (acccessed 2023/12/01).

(2) Medina-Sánchez, M.; Magdanz, V.; Guix, M.; Fomin, V. M.; Schmidt, O. G. Swimming Microrobots: Soft, Reconfigurable, and Smart. Advanced Functional Materials 2018, 28 (25), 1707228. DOI: https://doi.org/10.1002/adfm.201707228.

(3) JianFeng; Cho, S. K. Mini and Micro Propulsion for Medical Swimmers. Micromachines 2014, 5 (1), 97-113.

(4) Nelson, B. J.; Kaliakatsos, I. K.; Abbott, J. J. Microrobots for Minimally Invasive Medicine. Annual Review of Biomedical Engineering 2010, 12 (1), 55-85. DOI: 10.1146/annurev-bioeng-010510-103409.

(5) Li, J.; Esteban-Fernández de Ávila, B.; Gao, W.; Zhang, L.; Wang, J. Micro/nanorobots for biomedicine: Delivery, surgery, sensing, and detoxification. Science Robotics 2017, 2 (4), eaam6431. DOI: doi:10.1126/scirobotics.aam6431.

(6) Parmar, J.; Vilela, D.; Villa, K.; Wang, J.; Sánchez, S. Micro- and Nanomotors as Active Environmental Microcleaners and Sensors. Journal of the American Chemical Society 2018, 140 (30), 9317-9331. DOI: 10.1021/jacs.8b05762.

(7) Mallory, S. A.; Valeriani, C.; Cacciuto, A. An Active Approach to Colloidal Self-Assembly. Annual Review of Physical

Chemistry 2018, 69 (1), 59-79. DOI: 10.1146/annurev-physchem-050317-021237 (acccessed 2023/06/30).

(8) Soto, F.; Wang, J.; Deshmukh, S.; Demirci, U. Reversible Design of Dynamic Assemblies at Small Scales. Advanced Intelligent Systems 2021, 3 (4), 2000193, https://doi.org/10.1002/aisy.202000193. DOI: https://doi.org/10.1002/aisy.202000193 (acccessed 2023/06/30).

(9) Fei, W.; Gu, Y.; Bishop, K. J. M. Active colloidal particles at fluid-fluid interfaces. Current Opinion in Colloid & Interface Science 2017, 32, 57-68. DOI: https://doi.org/10.1016/j.cocis.2017.10.001.

(10) Ignés-Mullol, J.; Sagués, F. Experiments with active and driven synthetic colloids in complex fluids. Current Opinion in Colloid & Interface Science 2022, 62, 101636. DOI: https://doi.org/10.1016/j.cocis.2022.101636.

(11) Moran, J. L.; Posner, J. D. Phoretic Self-Propulsion. Annual Review of Fluid Mechanics 2017, 49 (1), 511-540. DOI: 10.1146/annurev-fluid-122414-034456.

(12) Zhang, Y.; Hess, H. Chemically-powered swimming and diffusion in the microscopic world. Nature Reviews Chemistry 2021, 5 (7), 500-510.

(13) Jang, B.; Ye, M.; Hong, A.; Wang, X.; Liu, X.; Bae, D.; Puigmartí Luis, J.; Pané, S. Catalytically Propelled Micro- and Nanoswimmers. Small Science 2023, 3 (11), 2300076. DOI: https://doi.org/10.1002/smsc.202300076.

(14) Wang, W.; Duan, W.; Ahmed, S.; Mallouk, T. E.; Sen, A. Small power: Autonomous nano- and micromotors propelled by self-generated gradients. Nano Today 2013, 8 (5), 531-554. DOI: https://doi.org/10.1016/j.nantod.2013.08.009.

(15) Robertson, B.; Huang, M.-J.; Chen, J.-X.; Kapral, R. Synthetic Nanomotors: Working Together through Chemistry. Accounts of Chemical Research 2018, 51 (10), 2355-2364. DOI: 10.1021/acs.accounts.8b00239.

(16) Dietrich, K.; Volpe, G.; Sulaiman, M. N.; Renggli, D.; Buttinoni, I.; Isa, L. Active Atoms and Interstitials in Two-Dimensional Colloidal Crystals. Physical Review Letters 2018, 120 (26), 268004. DOI: 10.1103/PhysRevLett.120.268004.

(17) Jalilvand, Z.; Haider, H.; Cui, J.; Kretzschmar; Ilona. Pt-SiO2 Janus Particles and the Water/Oil Interface: A Competition between Motility and Thermodynamics. Langmuir 2020, 36 (25), 6880-6887. DOI: 10.1021/acs.langmuir.9b03454.

(18) Palacios, L. S.; Katuri, J.; Pagonabarraga, I.; Sánchez, S. Guidance of active particles at liquid–liquid interfaces near surfaces. Soft Matter 2019, 15 (32), 6581-6588, 10.1039/C9SM01016E. DOI: 10.1039/C9SM01016E.

(19) Sharan, P.; Postek, W.; Gemming, T.; Garstecki, P.; Simmchen, J. Study of Active Janus Particles in the Presence of an Engineered Oil–Water Interface. Langmuir 2021, 37 (1), 204-210. DOI: 10.1021/acs.langmuir.0c02752.

(20) Xu, P.; Duan, S.; Xiao, Z.; Yang, Z.; Wang, W. Light-powered active colloids from monodisperse and highly tunable microspheres with a thin TiO2 shell. Soft Matter 2020, 16 (26), 6082-6090, 10.1039/D0SM00719F. DOI: 10.1039/D0SM00719F.

(21) Goia, D.; Matijević, E. Tailoring the particle size of monodispersed colloidal gold. Colloids and Surfaces A: Physicochemical and Engineering Aspects 1999, 146 (1), 139-152. DOI: https://doi.org/10.1016/S0927-7757(98)00790-0.

(22) Zhang, Q.; Dong, R.; Wu, Y.; Gao, W.; He, Z.; Ren, B. Light-Driven Au-WO3@C Janus Micromotors for Rapid Photodegradation of Dye Pollutants. ACS Applied Materials & Interfaces 2017, 9 (5), 4674-4683. DOI: 10.1021/acsami.6b12081.

(23) Lyu, X.; Liu, X.; Zhou, C.; Duan, S.; Xu, P.; Dai, J.; Chen, X.; Peng, Y.; Cui, D.; Tang, J.; et al. Active, Yet Little Mobility: Asymmetric Decomposition of H2O2 Is Not Sufficient in Propelling Catalytic Micromotors. Journal of the American Chemical Society 2021, 143 (31), 12154-12164. DOI: 10.1021/jacs.1c04501.

(24) Zhou, C.; Zhang, H. P.; Tang, J.; Wang, W. Photochemically Powered AgCl Janus Micromotors as a Model System to Understand Ionic Self-Diffusiophoresis. Langmuir 2018, 34 (10), 3289-3295. DOI: 10.1021/acs.langmuir.7b04301.

(25) Barnkob, R.; Rossi, M. General defocusing particle tracking: fundamentals and uncertainty assessment. Experiments in Fluids 2020, 61 (4), 110. DOI: 10.1007/s00348-020-2937-5.

(26) DeCamp, S. J.; Redner, G. S.; Baskaran, A.; Hagan, M. F.; Dogic, Z. Orientational order of motile defects in active nematics. Nature Materials 2015, 14 (11), 1110-1115. DOI: 10.1038/nmat4387.

(27) Xiao, Z.; Duan, S.; Xu, P.; Cui, J.; Zhang, H.; Wang, W. Synergistic Speed Enhancement of an Electric-Photochemical Hybrid Micromotor by Tilt Rectification. ACS Nano 2020, 14 (7), 8658-8667. DOI: 10.1021/acsnano.0c03022.

(28) Qian, H.; Sheetz, M. P.; Elson, E. L. Single particle tracking. Analysis of diffusion and flow in two-dimensional systems. Biophysical Journal 1991, 60 (4), 910-921. DOI: https://doi.org/10.1016/S0006-3495(91)82125-7.

(29) Daumas, F.; Destainville, N.; Millot, C.; Lopez, A.; Dean, D.; Salomé, L. Confined Diffusion Without Fences of a G-Protein-Coupled Receptor as Revealed by Single Particle Tracking. Biophysical Journal 2003, 84 (1), 356-366. DOI: https://doi.org/10.1016/S0006-3495(03)74856-5.

(30) Wang, W.; Mallouk, T. E. A Practical Guide to Analyzing and Reporting the Movement of Nanoscale Swimmers. ACS Nano 2021, 15 (10), 15446-15460. DOI: 10.1021/acsnano.1c07503.

(31) Liu, X.; Yang, S.; Lyu, X.; Liu, S.; Wang, Y.; Li, Y.; Wang, B.; Chen, W.; Wang, W.; Guo, J.; et al. Instant Preparation of Ultraclean Gold Nanothorns under Ambient Conditions for SERS Kit-Enabled Mobile Diagnosis. Analytical Chemistry 2021, 93 (49), 16628-16637. DOI: 10.1021/acs.analchem.1c04099.

(32) Bartolini, D.; Arato, I.; Mancuso, F.; Giustarini, D.; Bellucci, C.; Vacca, C.; Aglietti, M. C.; Stabile, A. M.; Rossi, R.; Cruciani, G.; et al. Melatonin modulates Nrf2 activity to protect porcine pre-pubertal Sertoli cells from the abnormal H(2) O(2) generation and reductive stress effects of cadmium. J Pineal Res 2022, 73 (1), e12806. DOI: 10.1111/jpi.12806 From NLM.

(33) Ajdari, A.; Bocquet, L. Giant Amplification of Interfacially Driven Transport by Hydrodynamic Slip: Diffusio-Osmosis and Beyond. Physical Review Letters 2006, 96 (18), 186102. DOI: 10.1103/PhysRevLett.96.186102.

(34) Schumb, W. C. Hydrogen peroxide; Reinhold Pub. Corp., 1955.

(35) Campbell, A. I.; Ebbens, S. J. Gravitaxis in Spherical Janus Swimming Devices. Langmuir 2013, 29 (46), 14066-14073. DOI: 10.1021/la403450j.

(36) Ebbens, S. J.; Howse, J. R. Direct Observation of the Direction of Motion for Spherical Catalytic Swimmers. Langmuir 2011, 27 (20), 12293-12296. DOI: 10.1021/la2033127.

(37) Howse, J. R.; Jones, R. A. L.; Ryan, A. J.; Gough, T.; Vafabakhsh, R.; Golestanian, R. Self-Motile Colloidal Particles: From Directed Propulsion to Random Walk. Physical Review Letters 2007, 99 (4), 048102. DOI: 10.1103/PhysRevLett.99.048102.

(38) Wang, W.; Lv, X.; Moran, J. L.; Duan, S.; Zhou, C. A practical guide to active colloids: choosing synthetic model systems for soft matter physics research. Soft Matter 2020, 16 (16), 3846-3868, 10.1039/D0SM00222D. DOI: 10.1039/D0SM00222D.

(39) Brown, A.; Poon, W. Ionic effects in self-propelled Pt-coated Janus swimmers. Soft Matter 2014, 10 (22), 4016-4027, 10.1039/C4SM00340C. DOI: 10.1039/C4SM00340C.

(40) Wheat, P. M.; Marine, N. A.; Moran, J. L.; Posner, J. D. Rapid Fabrication of Bimetallic Spherical Motors. Langmuir 2010, 26 (16), 13052-13055. DOI: 10.1021/la102218w.

(41) Dong, R.; Zhang, Q.; Gao, W.; Pei, A.; Ren, B. Highly Efficient Light-Driven TiO2–Au Janus Micromotors. ACS Nano 2016, 10 (1), 839-844. DOI: 10.1021/acsnano.5b05940.

(42) Gao, Y.; Dullens, R. P. A.; Aarts, D. G. A. L. Bulk synthesis of silver-head colloidal rodlike micromotors. Soft Matter 2018, 14 (35), 7119-7125, 10.1039/C8SM00832A. DOI: 10.1039/C8SM00832A.

(43) Shah, Z. H.; Wang, S.; Xian, L.; Zhou, X.; Chen, Y.; Lin, G.; Gao, Y. Highly efficient chemically-driven micromotors with controlled snowman-like morphology. Chemical Communications 2020, 56 (97), 15301-15304, 10.1039/D0CC06812H. DOI: 10.1039/D0CC06812H.

(44) Hong, Y.; Velegol, D.; Chaturvedi, N.; Sen, A. Biomimetic behavior of synthetic particles: from microscopic randomness to macroscopic control. Physical Chemistry Chemical Physics 2010, 12 (7), 1423-1435, 10.1039/B917741H. DOI: 10.1039/B917741H.

(45) Wittmann, M.; Popescu, M. N.; Domínguez, A.; Simmchen, J. Active spheres induce Marangoni flows that drive collective dynamics. The European Physical Journal E 2021, 44 (2), 15. DOI: 10.1140/epje/s10189-020-00006-5.

(46) Chanda, A.; Fokin, V. V. Organic Synthesis "On Water". Chemical Reviews 2009, 109 (2), 725-748. DOI: 10.1021/cr800448q.

(47) Wei, Z.; Li, Y.; Cooks, R. G.; Yan, X. Accelerated Reaction Kinetics in Microdroplets: Overview and Recent Developments. Annual Review of Physical Chemistry 2020, 71 (1), 31-51. DOI: 10.1146/annurev-physchem-121319-110654 (acccessed 2023/06/24).

(48) Narayan, S.; Muldoon, J.; Finn, M. G.; Fokin, V. V.; Kolb, H. C.; Sharpless, K. B. "On water": unique reactivity of organic compounds in aqueous suspension. Angew Chem Int Ed Engl 2005, 44 (21), 3275-3279. DOI: 10.1002/anie.200462883 From NLM.

(49) Gajewski, J. J.; Jurayj, J.; Kimbrough, D. R.; Gande, M. E.; Ganem, B.; Carpenter, B. K. The mechanism of rearrangement of chorismic acid and related compounds. Journal of the American Chemical Society 1987, 109 (4), 1170-1186. DOI: 10.1021/ja00238a029.

(50) Rideout, D. C.; Breslow, R. Hydrophobic acceleration of Diels-Alder reactions. Journal of the American Chemical Society 1980, 102 (26), 7816-7817. DOI: 10.1021/ja00546a048.

(51) Hao, H.; Leven, I.; Head-Gordon, T. Can electric fields drive chemistry for an aqueous microdroplet? Nature Communications 2022, 13 (1), 280. DOI: 10.1038/s41467-021-27941-x.

(52) Manjare, M.; Ting Wu, Y.; Yang, B.; Zhao, Y.-P. Hydrophobic catalytic Janus motors: Slip boundary condition and enhanced catalytic reaction rate. Applied Physics Letters 2014, 104 (5). DOI: 10.1063/1.4863952 (acccessed 6/24/2023).

(53) Calvo-Marzal, P.; Manesh, K. M.; Kagan, D.; Balasubramanian, S.; Cardona, M.; Flechsig, G.-U.; Posner, J.; Wang, J. Electrochemically-triggered motion of catalytic nanomotors. Chemical Communications 2009, (30), 4509-4511, 10.1039/B909227G. DOI: 10.1039/B909227G.

(54) Crowdy, D. G. Wall effects on self-diffusiophoretic Janus particles: a theoretical study. Journal of Fluid Mechanics 2013, 735, 473-498. DOI: 10.1017/jfm.2013.510 From Cambridge University Press Cambridge Core.

(55) Simmchen, J.; Katuri, J.; Uspal, W. E.; Popescu, M. N.; Tasinkevych, M.; Sánchez, S. Topographical pathways guide chemical microswimmers. Nature Communications 2016, 7 (1), 10598. DOI: 10.1038/ncomms10598.

(56) Das, S.; Garg, A.; Campbell, A. I.; Howse, J.; Sen, A.; Velegol, D.; Golestanian, R.; Ebbens, S. J. Boundaries can steer active Janus spheres. Nature Communications 2015, 6 (1), 8999. DOI: 10.1038/ncomms9999.

(57) Uspal, W. E.; Popescu, M. N.; Dietrich, S.; Tasinkevych, M. Self-propulsion of a catalytically active particle near a planar wall: from reflection to sliding and hovering. Soft Matter 2015, 11 (3), 434-438, 10.1039/C4SM02317J. DOI: 10.1039/C4SM02317J.

(58) Ketzetzi, S.; de Graaf, J.; Doherty, R. P.; Kraft, D. J. Slip Length Dependent Propulsion Speed of Catalytic Colloidal Swimmers near Walls. Physical Review Letters 2020, 124 (4), 048002. DOI: 10.1103/PhysRevLett.124.048002.

(59) Gu, Y.; Li, D. Measurements of Contact Angles between an Oil–Water Interface and a Fiber by the ACDPAC Technique. Journal of Colloid and Interface Science 1998, 206 (1), 288-296. DOI: https://doi.org/10.1006/jcis.1998.5670.

(60) Wei, M.; Zhou, C.; Tang, J.; Wang, W. Catalytic Micromotors Moving Near Polyelectrolyte-Modified Substrates: The Roles of Surface Charges, Morphology, and Released Ions. ACS Applied Materials & Interfaces 2018, 10 (3), 2249-2252. DOI: 10.1021/acsami.7b18399.

(61) Wang, W.; Chiang, T.-Y.; Velegol, D.; Mallouk, T. E. Understanding the Efficiency of Autonomous Nano- and Microscale Motors. Journal of the American Chemical Society 2013, 135 (28), 10557-10565. DOI: 10.1021/ja405135f.

(62) Gao, Q.; Yang, Z.; Zhu, R.; Wang, J.; Xu, P.; Liu, J.; Chen, X.; Yan, Z.; Peng, Y.; Wang, Y.; et al. Ultrasonic Steering Wheels: Turning Micromotors by Localized Acoustic Microstreaming. ACS Nano 2023, 17 (5), 4729-4739. DOI: 10.1021/acsnano.2c11070.

(63) Nishimori, H.; Suematsu, N. J.; Nakata, S. Collective Behavior of Camphor Floats Migrating on the Water Surface. Journal of the Physical Society of Japan 2017, 86 (10), 101012. DOI: 10.7566/JPSJ.86.101012 (acccessed 2023/06/24).

(64) Eastoe, J.; Dalton, J. S. Dynamic surface tension and adsorption mechanisms of surfactants at the air–water interface. Advances in Colloid and Interface Science 2000, 85 (2), 103-144. DOI: https://doi.org/10.1016/S0001-8686(99)00017-2.

(65) Dai, B.; Wang, J.; Xiong, Z.; Zhan, X.; Dai, W.; Li, C.-C.; Feng, S.-P.; Tang, J. Programmable artificial phototactic microswimmer. Nature Nanotechnology 2016, 11 (12), 1087-1092. DOI: 10.1038/nnano.2016.187.

(66) Duan, S.; Xu, P.; Wang, W. Better fuels for photocatalytic micromotors: a case study of triethanolamine. Chemical Communications 2021, 57 (77), 9902-9905, 10.1039/D1CC03857E. DOI: 10.1039/D1CC03857E.

(67) Kaiser, A.; Popowa, K.; Wensink, H. H.; Löwen, H. Capturing self-propelled particles in a moving microwedge. Physical Review E 2013, 88 (2), 022311. DOI: 10.1103/PhysRevE.88.022311.

(68) Liu, C.; Zhou, C.; Wang, W.; Zhang, H. P. Bimetallic Microswimmers Speed Up in Confining Channels. Physical Review Letters 2016, 117 (19), 198001. DOI: 10.1103/PhysRevLett.117.198001.

(69) Sridhar, V.; Podjaski, F.; Kröger, J.; Jiménez-Solano, A.; Park, B.-W.; Lotsch, B. V.; Sitti, M. Carbon nitride-based light-driven microswimmers with intrinsic photocharging ability. Proceedings of the National Academy of Sciences 2020, 117 (40), 24748-24756. DOI: 10.1073/pnas.2007362117 (acccessed 2023/06/24).

(70) Zhan, X.; Wang, J.; Xiong, Z.; Zhang, X.; Zhou, Y.; Zheng, J.; Chen, J.; Feng, S.-P.; Tang, J. Enhanced ion tolerance of electrokinetic locomotion in polyelectrolyte-coated microswimmer. Nature Communications 2019, 10 (1), 3921. DOI: 10.1038/s41467-019-11907-1.

(71) Feuerstein, L.; Biermann, C. G.; Xiao, Z.; Holm, C.; Simmchen, J. Highly Efficient Active Colloids Driven by Galvanic Exchange Reactions. Journal of the American Chemical Society 2021, 143 (41), 17015-17022. DOI: 10.1021/jacs.1c06400.